Pinning Effects of Exchange and Magnetocrystalline Anisotropies on Skyrmion Lattice

Xuejin Wan[1], Yangfan Hu[1,2]*, Zhipeng Hou[3] and Biao Wang[1,2]*

[1]School of Materials Science and Engineering, Dongguan University of Technology, Dongguan, China, [2]Sino-French Institute of Nuclear Engineering and Technology, Sun Yat-sen University, Zhuhai, China, [3]Guangdong Provincial Key Laboratory of Optical Information Materials and Technology and Institute for Advanced Materials, South China Academy of Advanced Optoelectronics, South China Normal University, Guangzhou, China

Reorientation of skyrmion crystal (SkX) with respect to crystallographic axes is believed to be insensitive to anisotropies of fourth order in spin-orbit coupling, for which sixth order terms are considered for explanation. Here, we show that this is wrong due to an oversimplified assumption that SkX possesses hexagonal symmetry. When the deformation of SkX is taken into account, fourth order anisotropies such as exchange anisotropy and magnetocrystalline anisotropy have pinning (in this work, the word 'pinning' refers to the reorientation effects of intrinsic anisotropy terms) effects on SkX. In particular, we reproduce some experiments of MnSi and $Fe_{1-x}Co_xSi$ by considering the effect of fourth order magnetocrystalline anisotropy alone. We reproduce the 30° rotation of SkX in Cu_2OSeO_3 by considering the combined effects of the exchange and magnetocrystalline anisotropies. And we use the exchange anisotropy to explain the reorientation of SkX in $VOSe_2O_5$.

Keywords: skyrmion crystal, pinning effect, exchange anisotropy, magnetocrystalline anisotropy, helimagnet

1 INTRODUCTION

Helimagnets have attracted extensive interest since the first observation of magnetic skyrmions in 2009 [1]. Magnetic skyrmions in helimagnets are nontrivial spin textures, in which the spins point in all of the directions wrapping a sphere. Their topological protection [2] and facile current driven motion [3, 4] make them possible to be applied in novel spintronic and information storage devices [5, 6].

In helimagnets such as MnSi, $Fe_{1-x}Co_xSi$, and Cu_2OSeO_3, the ferromagnetic exchange interaction (for Cu_2OSeO_3, the exchange interaction consists of ferromagnetic and antiferromagnetic interactions, but the field-induced ground state is closer to ferromagnetic than antiferromagnetic [7, 8]) and the Dzyaloshinsky-Moriya interaction (DMI), which arises due to the broken of space inversion symmetry [9, 10], dominate the free energy when studying bulk material free from any external magnetic field. The former favors parallel spin alignment, while the latter favors the twist of the spins. They compete with each other and result in SkX at appropriate magnetic field just below the Curie temperature [1, 11–14]. In experiments, when the magnetic field is along directions with high symmetry, such as the [001], [111] and [110] directions, the wave vectors of SkX are orientated with respect to the crystallographic axes [1, 12, 15, 16]. This indicates the existence of anisotropy energy. The anisotropies of fourth order in spin-orbit coupling, such as the exchange anisotropy and fourth order magnetocrystalline anisotropy, are widely used to explain the pinning of helical phase, the transition from helical to conical phase and the appearance of tilted conical phase [1, 17–20]. However, according to the perturbation theory [1, 12, 16, 21], which treats the anisotropies

perturbatively and approximates SkX by a triple-Q structure with three equivalent wave vectors forming a regular triangle, they are insensitive to the pinning of SkX. As a consequence, anisotropies with higher order are proposed. In our opinion, ignoring the deformation of SkX is oversimplified, because many experiments show that the structure of SkX is sensitive to anisotropy of the system which destroys its hexagonal symmetry [22–24].

In this work, we study the pinning effects of the exchange anisotropies and the fourth order magnetocrystalline anisotropy on deformable SkX. We apply a rescaled free-energy-density model for T point group and describe Bloch SkX by a three-order Fourier expansion with deformation-related degrees of freedom. Firstly, we study four anisotropies (three types of exchange anisotropies and a fourth order magnetocrystalline anisotropy in helimagnets with T symmetry) separately. It is found that they have different pinning effects on SkX. Then, by plotting the deformation-related parameters as functions of one exchange anisotropy, we figure out that the deformation of SkX is characterized by the change of amplitudes, lengths and azimuth angles of wave vectors. Next, we compare our results with some experiments, the fourth order magnetocrystalline anisotropy may explain the pinning of SkX in MnSi [1, 25, 26] and $Fe_{1-x}Co_xSi$ [12, 27–29]. To reproduce the 30° rotation of SkX in Cu_2OSeO_3 [16], we consider both the exchange and magnetocrystalline anisotropy, and find that at certain conditions 30° rotation of SkX occurs when temperature or magnetic field changes. Lastly, we expand our model so that it is applicable to C_{nv} helimagnets hosting Néel SkX. It is found that exchange anisotropy has pinning effects on Néel SkX in C_{4v} helimagnets but not in C_{3v} or C_{6v} helimagnets.

2 MODEL

Based on the continuum spin model established by Bak and Jensen [17], we write the rescaled free-energy density [30] for helimagnets with the symmetry of T point group in the following form:

$$\omega(\mathbf{m}) = \sum_{i=1}^{3}\left(\frac{\partial \mathbf{m}}{\partial r_i}\right)^2 + 2\mathbf{m}\cdot(\nabla\times\mathbf{m}) - 2\mathbf{b}\cdot\mathbf{m} + \omega_L(\mathbf{m}) + \omega_a(\mathbf{m}).$$
(1)

Here, $\mathbf{m}$ is the rescaled magnetization. The first two terms in **Eq. (1)** represent the ferromagnetic exchange interaction and the DMI, respectively. The third term is the Zeeman energy under the rescaled magnetic field $\mathbf{b}$. $\omega_L = t\mathbf{m}^2 + \mathbf{m}^4$ is the Landau expansion with the rescaled temperature t, it consists of the second and the fourth order terms. The last term ω_a is the anisotropy energy. In this work, we consider only the exchange anisotropy and the fourth order magnetocrystalline anisotropy, and we express ω_a as

$$\omega_a = a_{e1}\sum_{i=1}^{3}\left(\frac{\partial m_i}{\partial r_i}\right)^2 + a_{e2}\sum_{i=1}^{3}\left(\frac{\partial m_i}{\partial r_{i+1}}\right)^2 + a_{e3}\sum_{i=1}^{3}\left(\frac{\partial m_i}{\partial r_{i-1}}\right)^2$$
$$+ a_m\sum_{i=1}^{3} m_i^4,$$
(2)

where a_{e1}, a_{e2} and a_{e3} are the coefficients of exchange anisotropy, a_m is the coefficient of magnetocrystalline anisotropy, r_{3+1} and r_{1-1} represent r_1 and r_3, respectively.

For bulk B20 materials, the skyrmion plane rotates with respect to the applied magnetic field. To describe the configuration of SkX under magnetic field with different direction, we should choose an appropriate cartesian coordinates system $O\text{-}r_1^*r_2^*r_3^*$ in which the magnetic field is along the r_3^* axis. Let the azimuthal and polar angles that characterize the magnetic field $\mathbf{b}$ be θ and ψ, respectively. We rotate $O\text{-}r_1r_2r_3$ counterclockwise about the r_3 axis by angle θ, and get a new cartesian coordinates system $O\text{-}r_1'r_2'r_3'$. We then perform a second rotation, this time about the r_2' axis by angle ψ, and we get the final cartesian coordinates system $O\text{-}r_1^*r_2^*r_3^*$ [**Figure 1**]. In terms of 3×3 orthogonal matrices, the product of the two operations can be written as $R(\theta,\psi) = R_{r_2'}(\psi)R_{r_3}(\theta)$. Due to the relation $R_{r_2'}(\psi) = R_{r_3}(\theta)R_{r_2}(\psi)R_{r_3}^{-1}(\theta)$, we have

$$R(\theta,\psi) = R_{r_3}(\theta)R_{r_2}(\psi)$$
$$= \begin{bmatrix} \cos\theta & -\sin\theta & 0 \\ \sin\theta & \cos\theta & 0 \\ 0 & 0 & 1 \end{bmatrix} \begin{bmatrix} \cos\psi & 0 & \sin\psi \\ 0 & 1 & 0 \\ -\sin\psi & 0 & \cos\psi \end{bmatrix}$$
(3)

In the cartesian coordinates system $O\text{-}r_1^*r_2^*r_3^*$, we apply the n-order Fourier decomposition to describe the magnetization texture of SkX [31],

$$\mathbf{m}^* = \mathbf{m}_0 + \sum_{i=1}^{n}\sum_{j=1}^{n_i} \mathbf{m}_{\mathbf{q}_{ij}} e^{i\mathbf{q}_{ij}^d \cdot \mathbf{r}^*}.$$
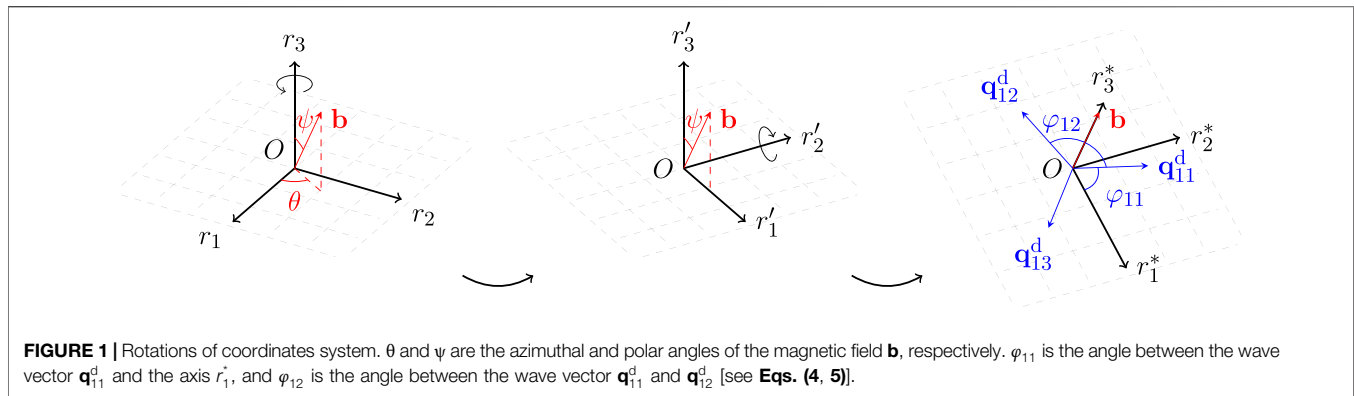(4)

Here, $\mathbf{m}_0 = [m_{01}, m_{02}, m_{03}]^T$ is the average magnetization over the entire SkX, and n_i is the number of nth order waves. The ith order waves are characterized by their wave vectors $\mathbf{q}_{ij}^d$ and polarizations $\mathbf{m}_{\mathbf{q}_{ij}}$. In the presence of anisotropy energy, SkX with hexagonal symmetry will go through deformation, and the deformation-related parameters are introduced through the following equation

$$\mathbf{q}_{ij}^d = \begin{bmatrix} 1+\varepsilon_{11}^q & \varepsilon_{12}^q + \omega^q \\ \varepsilon_{12}^q - \omega^q & 1+\varepsilon_{22}^q \end{bmatrix} \mathbf{q}_{ij}.$$
(5)

In reciprocal space, ε_{11}^q and ε_{22}^q are the normal strains; ε_{12}^q and ω^q reflect the shear deformation and rotation of the plane spanned by $\mathbf{q}_{ij}^d$, respectively. $\mathbf{q}_{ij}$ are the undeformed wave vectors, they all can be expressed as a linear combination of $\mathbf{q}_{11}$ and $\mathbf{q}_{12}$ (without loss of generality, for hexagonal SkX, we set $\mathbf{q}_{11} = [0, 1]^T$, $\mathbf{q}_{12} = \left[-\frac{\sqrt{3}}{2}, -\frac{1}{2}\right]^T$). As to $\mathbf{m}_{\mathbf{q}_{ij}}$, we decompose them along the basis vectors $\mathbf{P}_{ij1} = \frac{1}{\sqrt{2}|\mathbf{q}_{ij}|}[-iq_{ijy}, iq_{ijx}, |\mathbf{q}_{ij}|]^T$, $\mathbf{P}_{ij2} = \frac{1}{|\mathbf{q}_{ij}|}[q_{ijx}, q_{ijy}, 0]^T$, and $\mathbf{P}_{ij3} = \frac{1}{\sqrt{2}|\mathbf{q}_{ij}|}[iq_{ijy}, -iq_{ijx}, |\mathbf{q}_{ij}|]^T$ (for the chosen of the orthogonal basis, see Ref. [32]), and we have

$$\mathbf{m}_{\mathbf{q}_{ij}} = \sum_{k=1}^{3} c_{ijk}\mathbf{P}_{ijk},$$
(6)

where $c_{ijk} = c_{ijk}^{re} + ic_{ijk}^{im}$ ($k = 1, 2, 3$) are the complex coefficients.

FIGURE 1 | Rotations of coordinates system. θ and ψ are the azimuthal and polar angles of the magnetic field **b**, respectively. φ_{11} is the angle between the wave vector $\mathbf{q}_{11}^d$ and the axis r_1^*, and φ_{12} is the angle between the wave vector $\mathbf{q}_{11}^d$ and $\mathbf{q}_{12}^d$ [see **Eqs. (4, 5)**].

According to **Eqs. (1)** and **(2)**, the free energy density is a functional of m_i and $m_{j,k}$ ($m_{j,k}$ denotes $\frac{\partial m_j}{\partial r_k}$), i.e., $\omega = \omega(m_i, m_{j,k})$. Applying the following coordinate transformation

$$m_i = \sum_{i'=1}^{3} R(\theta, \psi)_{ii'} m_{i'}^*, \qquad (7)$$

$$m_{j,k} = \sum_{j',k'=1}^{3} R(\theta, \psi)_{jj'} R(\theta, \psi)_{kk'} m_{j',k'}^*, \qquad (8)$$

the free-energy density can be rewritten as, after averaging over a magnetic unit cell

$$\omega = \omega\left(\varepsilon_{11}^q, \varepsilon_{22}^q, \varepsilon_{12}^q, \omega_{11}^q, m_{01}, m_{02}, m_{03}, c_{ijk}^{re}, c_{ijk}^{im}\right). \qquad (9)$$

At certain temperature t, magnetic field **b**, rotation angles θ and ψ, exchange and magnetocrystalline anisotropies a_{e1}, a_{e2}, a_{e3} and a_m, the parameters describing SkX are calculated *via* minimization of **Eq. (9)**. In this work, we set the order of Fourier expansion $n = 3$.

Our analytical method can only deal with periodic magnetization structure. For the cases where the periodicity of skyrmions is broken, e.g., the thermal-induced disorder or the pinning from impurities, the review [33] and references therein are good to refer to.

3 RESULTS AND DISCUSSION

We first investigate the pinning effects of anisotropies a_{e1}, a_{e2}, a_{e3} and a_m on Bloch SkX, separately. The value of θ is 45°; thus, $\psi = 0°$, 55° and 90° correspond to the directions [001], [111] and [110], respectively. The temperature and the magnetic field are set to be $t = 0.5$ and $\mathbf{b} = [0, 0, 0.2]^T$ (in the O-$r_1^* r_2^* r_3^*$ coordinate system) so that SkX exists as a stable or metastable state. The thermodynamic parameters for MnSi [34] and Cu_2OSeO_3 [7] are available. Using these parameters, we have $(T, B) = (28.0K, 87mT)$ for MnSi and $(T, B) = (58.1K, 4.3mT)$ for Cu_2OSeO_3, these points are near the skyrmion stable region in the magnetic field-temperature phase diagram. The anisotropy coefficients of helimagnets are hard to get in experiments. We only find the relative exchange anisotropy for GaV_4O_8, which is about 5% [35]. In this work, the values used for the anisotropy

coefficients are 0.005 ~ 0.1. We think, to some extent, the values are within a realistic range.

We change the rotation-related parameter ω^q, minimize the free energy density and then plot ω as a function of φ_{11}, the angle between the wave vector $\mathbf{q}_{11}^d$ and the r_1^* axis, in **Figure 2**. **Figures 2A,B** show the effects of exchange anisotropy a_{e1} on SkX. For **b**||[001], a negative a_{e1} (**Figure 2A**) prefers a wave vector along the [100] or [010] direction; while a positive a_{e1} (**Figure 2B**) prefers a wave vector along the [110] or [1$\bar{1}$0] direction. For **b**||[111] and [110], ω reaches its minimum at $\varphi_{11} = 90°$ and $\varphi_{11} = 60°$, respectively (**Figures 2A,B**), i.e., both negative and positive a_{e1} prefer a wave vector along the [110] direction for **b**||[111], and along the [001] direction for **b**||[110]. **Figures 1C–F** show the effects of a_{e2} and a_{e3} on SkX, respectively. For **b**||[001], a a_{e2}, no matter what its sign is, pins a wave vector of SkX along the [010] direction; while a a_{e3} pins a wave vector of SkX along the [100] direction. For **b**||[111], φ_{11} is between 45° and 60° or between 60° and 75°, meaning that no wave vector is along any direction with high symmetry. For **b**||[110], both a_{e2} and a_{e3} pin a wave vector of SkX along the [001] direction. **Figures 2G,H** show the effects of a_m on SkX. For **b**||[001] and [111] , a_m has the same the pinning effects on SkX as a_{e1}; while for **b**||[110], a_m is different from a_{e1}, it results in a wave vector along the [110] direction.

In **Figure 2**, we give the values of $\Delta\omega$, difference between the maximum and minimum of free energy. They are much smaller than ω (about −0.1), about 10^{-9} for $a_m = \pm 0.05$ and $\psi = 0°$, and about 10^{-7}-10^{-5} for other cases. The strength of a_m-induced anisotropy in (001) plane is obviously smaller than that in (111) and (110) planes. Comparing the energy curves for a_{e2} and for a_{e3}, we find that they have the same $\Delta\omega$ and are symmetric about $\varphi_{11} = 60°$. The similarity between a_{e2} and a_{e3} can be inferred from their energy formula in **Eq. 2**, which are related by the coordinate transformation $r_1 \leftrightarrow r_2$. It should be noticed that for **b**||[001], the periodicity of $\omega(\varphi_{11})$ is 30° for a_{e1} and a_m, and is 60° for a_{e2} and a_{e3}. This can be explained by symmetry analysis. The a_{e1} and a_m terms in **Eq. (2)** have a higher symmetry than T point group, they are invariant with respect to fourfold C_4 rotations around the $\langle 001 \rangle$ axes. a_{e1} and a_m terms in **Eq. (2)** have lower symmetry and are invariant with respect ot twofold C_2 rotations around the $\langle 001 \rangle$ axes, meaning the broken of the equivalence between [100] and [010].
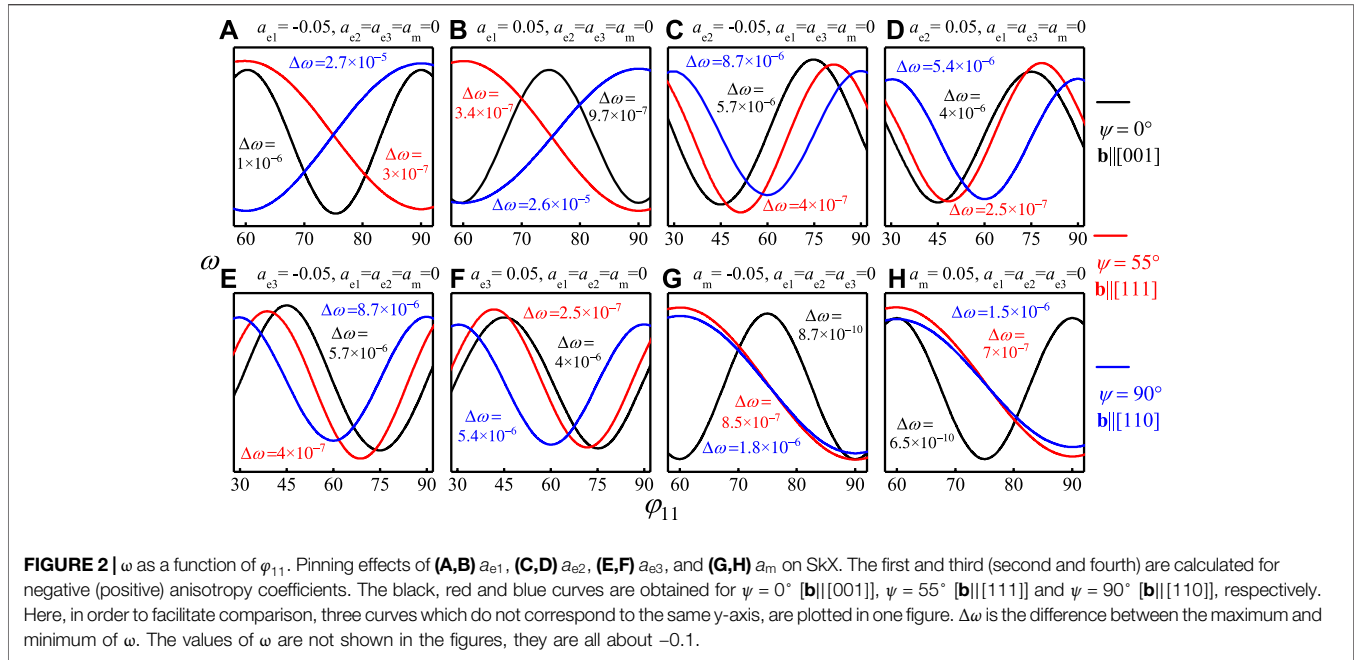
FIGURE 2 | ω as a function of φ_{11}. Pinning effects of **(A,B)** a_{e1}, **(C,D)** a_{e2}, **(E,F)** a_{e3}, and **(G,H)** a_m on SkX. The first and third (second and fourth) are calculated for negative (positive) anisotropy coefficients. The black, red and blue curves are obtained for $\psi = 0°$ [**b**||[001]], $\psi = 55°$ [**b**||[111]] and $\psi = 90°$ [**b**||[110]], respectively. Here, in order to facilitate comparison, three curves which do not correspond to the same y-axis, are plotted in one figure. $\Delta\omega$ is the difference between the maximum and minimum of ω. The values of ω are not shown in the figures, they are all about -0.1.
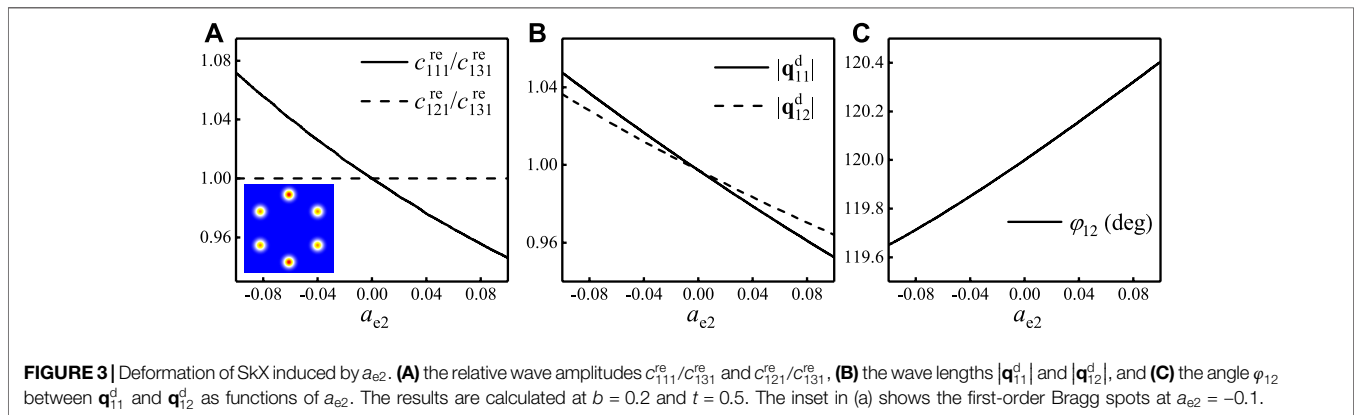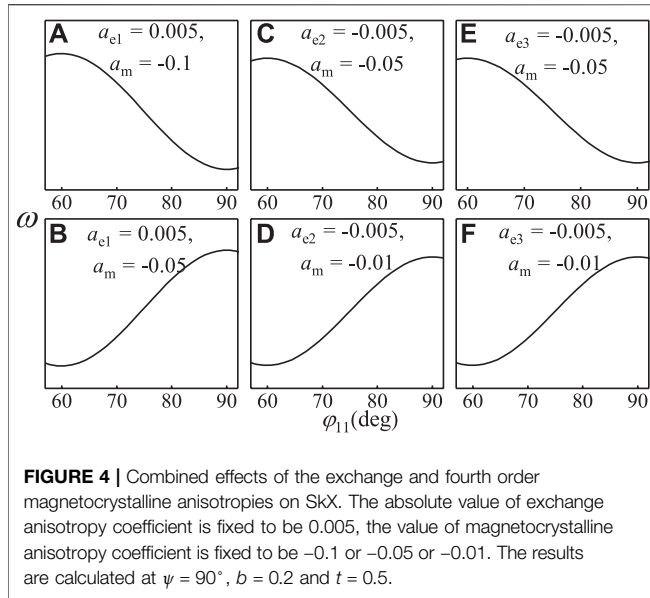

FIGURE 3 | Deformation of SkX induced by a_{e2}. **(A)** the relative wave amplitudes $c_{111}^{re}/c_{131}^{re}$ and $c_{121}^{re}/c_{131}^{re}$, **(B)** the wave lengths $|\mathbf{q}_{11}^d|$ and $|\mathbf{q}_{12}^d|$, and **(C)** the angle φ_{12} between $\mathbf{q}_{11}^d$ and $\mathbf{q}_{12}^d$ as functions of a_{e2}. The results are calculated at $b = 0.2$ and $t = 0.5$. The inset in (a) shows the first-order Bragg spots at $a_{e2} = -0.1$.

SkX is treated as a deformable structure. To reveal how anisotropy energy deforms SkX, we take a_{e2} as an example and plot some deformation-related parameters as functions of a_{e2} in **Figure 3**. It can be found that for nonzero a_{e2}, 1) the wave amplitudes $c_{111}^{re} \neq c_{131}^{re}$ (**Figure 3A**), 2) the wave lengths of $\mathbf{q}_{11}^d$ and $\mathbf{q}_{12}^d$ are not equal to each other (**Figure 3B**), and 3) the angle φ_{12} between $\mathbf{q}_{11}^d$ and $\mathbf{q}_{12}^d$ deviates from 120° (**Figure 3C**). We conclude that anisotropy energy breaks the hexagonal symmetry of SkX by changing the amplitudes of, the lengths of, and the angles between the wave vectors. In many of the small-angle neutron scattering (SANS) experiments (1; 27; 36), the observed Bragg spots have different intensities, this might be explained by our calculation. By energy minimization, we find that the dominant coefficients c_{ijk} are c_{111}^{re}, c_{121}^{re} and c_{131}^{re}, which represent the wave amplitudes of the first order waves with vectors $\mathbf{q}_{11}^d$, $\mathbf{q}_{12}^d$ and $\mathbf{q}_{13}^d$. Their ratios reflect the relative intensities of the first-order Bragg spots. In the inset of the

Figure 3A, two Bragg spots are brighter than the other four, because $c_{131}^{re} = c_{121}^{re} < c_{111}^{re}$.

We now compare our results with some experiments. The SANS experiments of $Fe_{1-x}Co_xSi$ [12, 27–29] show that for **b**||[111] and [110] directions, two of the six scattering spots are aligned with the [1$\bar{1}$0] axis; for **b**||[001], two sets of six scattering spots are observed, one is aligned with one the [100] direction, the other one the [010] direction. This is compatible with the results shown in **Figure 2G**. Therefore, a negative a_m may explain the pinning of SkX in $Fe_{1-x}Co_xSi$. Different from $Fe_{1-x}Co_xSi$, MnSi [26] is observed to have a wave vector along the [110] direction for **b**||[001]. This may be explained by a positive a_m (**Figure 2H**. We should point out that at zero magnetic field, a negative (positive) a_m prefers the $\langle 100 \rangle$ ($\langle 111 \rangle$) directions for the helical state, which is indeed the case for $Fe_{1-x}Co_xSi$ (MnSi) [1, 28, 29, 37, 38]. In the work [26], two kinds of sixth order magnetocrystalline anisotropies $\mathbf{m}$ ·

FIGURE 4 | Combined effects of the exchange and fourth order magnetocrystalline anisotropies on SkX. The absolute value of exchange anisotropy coefficient is fixed to be 0.005, the value of magnetocrystalline anisotropy coefficient is fixed to be −0.1 or −0.05 or −0.01. The results are calculated at $\psi = 90°$, $b = 0.2$ and $t = 0.5$.

$(\partial_{r_1}^6 + \partial_{r_2}^6 + \partial_{r_3}^6)\mathbf{m}$ and $\mathbf{m} \cdot (\partial_{r_1}^4 \partial_{r_2}^2 + \partial_{r_2}^4 \partial_{r_3}^2 + \partial_{r_3}^4 \partial_{r_1}^2)\mathbf{m}$ are thought to be responsible for the pinning of SkX in MnSi. However, this is contrary to other works [12, 21] which show that the second sixth order magnetocrystalline anisotropy determines the reorientation of SkX for $\mathbf{b}||[001]$ and it pins SkX with a wave vector along the [010] or [100] direction depending on the sign of its coefficient. The SANS experiments of MnSi in Ref. [26] can not be explained by the sixth order magnetocrystalline anisotropies.

Cu_2OSeO_3 is another helimagnet hosting SkX, a peculiar experimental phenomenon about it is that for $\mathbf{b}||[110]$, SkX is reorientated with a wave vector along the $[1\bar{1}0]$ or [001] direction depending on the temperature and magnetic field conditions [16]. To explain this, we should consider the exchange and fourth order magnetocrystalline anisotropies at the same time. As a first step, we determine the signs of anisotropies $a_{e1} > 0$, $a_{e2} < 0$, $a_{e3} < 0$ and $a_m < 0$ according to the fact that [100] is an easy axis for the helical state at zero field [20, 39, 40]. Then we confirm by **Figure 4** that for $\mathbf{b}||[110]$, a "dominant" magnetocrystalline anisotropy pins SkX with a wave vector along the [001] direction, while a "dominant" exchange anisotropy pins SkX with a wave vector along the $[1\bar{1}0]$ direction. Here, the word "dominant" depends on the type of exchange anisotropy considered. When $a_m = −0.05$, the "dominant" anisotropy is a_{e1} for $a_{e1} = 0.005$ (**Figures 4A,B**), and is a_m for $a_{e2} = −0.005$ or $a_{e3} = −0.005$ (**Figures 4C–F**). Lastly, we take the temperature and magnetic field into account and try to reproduce the 30° rotation of SkX in Cu_2OSeO_3. The anisotropies we considered are a_{e1} and a_m, and their values are 0.005 and −0.1, respectively, the same as that for **Figure 4A**. We fix the magnetic field $b = 0.2$ and change the temperature from 0.5 to 0.8 (**Figure 5A**). It is found that the angle φ_{11}^*, for which the free energy reaches its minimum, drops suddenly from 90° to 60° at $t = 0.66$. Then we fix the temperature $t = 0.65$ and change the magnetic field from 0.15 to 0.27 [**Figure 5B**]. Similar phenomenon is observed, φ_{11}^* drops from 90° to 60° at $b = 0.21$. Our results agree with the experiments of Cu_2OSeO_3 [16].

In another published work [41], we explain the electric-field-induced continuous rotation of SkX [42] by extending the present model. Unlike a previous theory [42] which explains the phenomenon by considering both the fourth and sixth order magnetocrystalline anisotropies, we find that a combination of fourth order exchange anisotropies and magnetocrystalline anisotropies dominates the phenomena. This is because the theory used in [42] obtains a positive coefficient of the fourth order magnetocrystalline anisotropy a_m which is inconsistent with other experiments [20, 39, 40], while our model obtains a negative a_m.
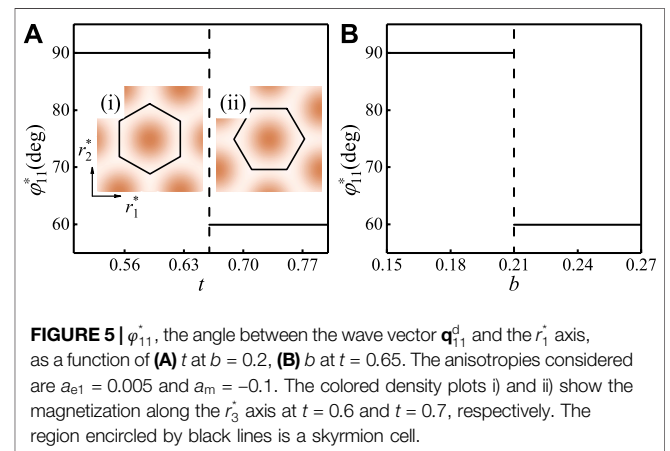
In polar magnets with C_{nv} ($n = 3, 4, 6$) symmetry, the DMI and the exchange anisotropy are different from that in **Eq. (1)**. By applying the symmetry analysis, we derive the DMI: $\omega_{DM} = 2m_1m_{3,1} − 2m_3m_{1,1} + 2m_2m_{3,2} − 2m_3m_{2,2}$ (in this case, the Néel SkX is stabilized, and the basis vectors in **Eq. (6)** are chosen to be
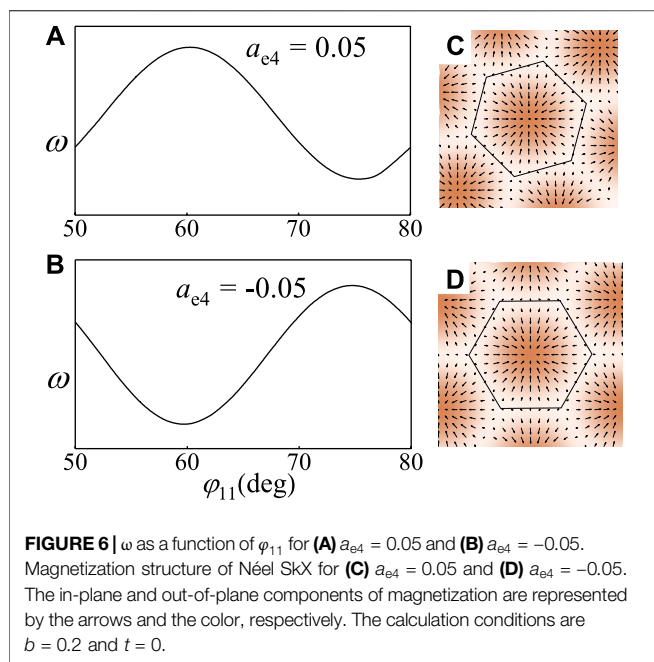
$\mathbf{P}_{ij1} = \frac{1}{\sqrt{2}|\mathbf{q}_{ij}|}[−iq_{ijx}, −iq_{ijy}, |\mathbf{q}_{ij}|]^T$, $\mathbf{P}_{ij2} = \frac{1}{|\mathbf{q}_{ij}|}[−q_{ijy}, q_{ijx}, 0]^T$, and $\mathbf{P}_{ij3} = \frac{1}{\sqrt{2}|\mathbf{q}_{ij}|}[iq_{ijx}, iq_{ijy}, |\mathbf{q}_{ij}|]^T$ [32]), and the exchange anisotropy:

$$\omega_{ea} = a_{e4}\left(\left(\frac{\partial m_2}{\partial r_1}\right)^2 + \left(\frac{\partial m_1}{\partial r_2}\right)^2\right) + a_{e5}\left(\left(\frac{\partial m_3}{\partial r_1}\right)^2 + \left(\frac{\partial m_3}{\partial r_2}\right)^2\right)$$

(10)

Here, we have ignored the terms $(\partial m_i/\partial r_3)^2$ due to the fact that in polar magnets, SkX plane is perpendicular to the n-fold axis no matter what direction the applied magnetic field is along [43, 44]. The term with coefficient a_{e5} is rotationally symmetric, and it has no pinning effects on SkX.

For C_{3v} and C_{6v} point groups, a_{e4} is zero. As a result, the orientation of the wave vector of SkX is insensitive to the exchange anisotropy. In Ref. [44], based on a discrete model and Monte Carlo simulations, the authors attribute the pinning of Néel SkX in C_{3v} polar magnet GaV_4Se_8 to the Dzyaloshinskii-Moriya vectors. However, according to the continuum model, the DMI possesses rotational symmetry and has no pinning effects on Néel SkX. In our opinion, this contradiction is because the

FIGURE 5 | φ_{11}^*, the angle between the wave vector $\mathbf{q}_{11}^d$ and the r_1^* axis, as a function of **(A)** t at $b = 0.2$, **(B)** b at $t = 0.65$. The anisotropies considered are $a_{e1} = 0.005$ and $a_m = −0.1$. The colored density plots i) and ii) show the magnetization along the r_3^* axis at $t = 0.6$ and $t = 0.7$, respectively. The region encircled by black lines is a skyrmion cell.

FIGURE 6 | ω as a function of φ_{11} for **(A)** $a_{e4} = 0.05$ and **(B)** $a_{e4} = -0.05$. Magnetization structure of Néel SkX for **(C)** $a_{e4} = 0.05$ and **(D)** $a_{e4} = -0.05$. The in-plane and out-of-plane components of magnetization are represented by the arrows and the color, respectively. The calculation conditions are $b = 0.2$ and $t = 0$.

continuum model ignores higher order DMI terms which emerge during the process of transforming the discrete model to the continuum model. These higher order DMI terms possess lower symmetry C_{3v} or C_{6v} and might reorientate Néel SkX.

For C_{4v} point groups, we have $a_{e4} \neq 0$. The term with coefficient a_{e4} will deform and thus reorientate the Néel SkX. Because it possesses C_{4v} symmetry, which is different from the C_{3v} symmetry possessed by the undeformed SkX. To study the pinning effects of a_4 on Néel SkX, we plot ω as a function of φ_{11} for 1) positive and 2) negative a_{e4} in **Figure 6**. It is found that a positive a_{e4} prefers a wave vector along the [110] or [1$\bar{1}$0] direction, and a negative a_{e4} prefers a wave vector along the [100] or [0$\bar{1}$0] direction. In experiments, very few C_{4v} helimagnets hosting Néel SkX have been found. VOSe$_2$O$_5$ [45] is one of these C_{4v} helimagnets, in which the Néel SkX is orientated with a wave vector along the [100] or [0$\bar{1}$0] direction. In previous theories, less attention has been paid to the reorientation of Néel SkX in C_{4v}

helimagnets. Here, a negative a_{e4} gives a possible explanation for the SkX-reorientation-related phenomena in VOSe$_2$O$_5$.

4 CONCLUSION

In conclusion, the exchange and fourth order magnetocrystalline anisotropies deform SkX by changing the amplitudes of, the lengths of, and the angles between wave vectors and thus show pinning effects on SkX. The results of magnetocrystalline anisotropy [exchange anisotropy] may explain some experiments of MnSi and Fe$_{1-x}$Co$_x$Si [VOSe$_2$O$_5$]. By considering the exchange and magnetocrystalline anisotropies at the same time, the 30° rotation of SkX in Cu$_2$OSeO$_3$ is reproduced.

DATA AVAILABILITY STATEMENT

The original contributions presented in the study are included in the article/Supplementary Material, further inquiries can be directed to the corresponding authors.

AUTHOR CONTRIBUTIONS

XW and YH conceived the idea. XW finished the analytical deduction, and performed all the calculations. XW, YH, ZH, and BW discussed the results for revision and co-wrote the manuscript.

FUNDING

REFERENCES

1. Mühlbauer S, Binz B, Jonietz F, Pfleiderer C, Rosch A, Neubauer A, et al. Skyrmion Lattice in a Chiral Magnet. *Science* (2009) 323:915–9. doi:10.1126/science.1166767

2. Nagaosa N, and Tokura Y. Topological Properties and Dynamics of Magnetic Skyrmions. *Nat Nanotech* (2013) 8:899–911. doi:10.1038/nnano.2013.243

3. Jonietz F, Mühlbauer S, Pfleiderer C, Neubauer A, Münzer W, Bauer A, et al. Spin Transfer Torques in Mnsi at Ultralow Current Densities. *Science* (2010) 330:1648–51. doi:10.1126/science.1195709

4. Yu XZ, Kanazawa N, Zhang WZ, Nagai T, Hara T, Kimoto K, et al. Skyrmion Flow Near Room Temperature in an Ultralow Current Density. *Nat Commun* (2012) 3:988. doi:10.1038/ncomms1990

5. Zhang X, Ezawa M, and Zhou Y. Magnetic Skyrmion Logic gates: Conversion, Duplication and Merging of Skyrmions. *Sci Rep* (2015a) 5:9400. doi:10.1038/srep09400

6. Zhang X, Zhao GP, Fangohr H, Liu JP, Xia WX, Xia J, et al. Skyrmion-skyrmion and Skyrmion-Edge Repulsions in Skyrmion-Based Racetrack Memory. *Sci Rep* (2015b) 5:7643. doi:10.1038/srep07643

7. Janson O, Rousochatzakis I, Tsirlin AA, Belesi M, Leonov AA, Rößler UK, et al. The Quantum Nature of Skyrmions and Half-Skyrmions in Cu2oseo3. *Nat Commun* (2014) 5:5376–11. doi:10.1038/ncomms6376

8. Yang JH, Li ZL, Lu XZ, Whangbo M-H, Wei S-H, Gong XG, et al. Strong Dzyaloshinskii-Moriya Interaction and Origin of Ferroelectricity inCu2OSeO3. *Phys Rev Lett* (2012) 109:107203. doi:10.1103/physrevlett.109.107203

9. Dzyaloshinsky I. A Thermodynamic Theory of "weak" Ferromagnetism of Antiferromagnetics. *J Phys Chem Sol* (1958) 4:241–55. doi:10.1016/0022-3697(58)90076-3

10. Moriya T. Anisotropic Superexchange Interaction and Weak Ferromagnetism. *Phys Rev* (1960) 120:91–8. doi:10.1103/physrev.120.91

11. Wilhelm H, Baenitz M, Schmidt M, Rößler UK, Leonov AA, and Bogdanov AN. Precursor Phenomena at the Magnetic Ordering of the Cubic Helimagnet Fege. *Phys Rev Lett* (2011) 107:127203. doi:10.1103/physrevlett.107.127203

12. Münzer W, Neubauer A, Adams T, Mühlbauer S, Franz C, Jonietz F, et al. Skyrmion Lattice in the Doped Semiconductor Fe1-Xcoxsi. *Phys Rev B* (2010) 81:041203. doi:10.1103/physrevb.81.041203

13. Ruff E, Widmann S, Lunkenheimer P, Tsurkan V, Bordács S, Kézsmárki I, et al. Multiferroicity and Skyrmions Carrying Electric Polarization in Gav4s8. *Sci Adv* (2015) 1:e1500916. doi:10.1126/sciadv.1500916

14. Omrani A, White J, Prša K, Živković I, Berger H, Magrez A, et al. Exploration of the Helimagnetic and Skyrmion Lattice Phase Diagram in Cu2oseo3 Using Magnetoelectric Susceptibility. *Phys Rev B* (2014) 89:064406. doi:10.1103/physrevb.89.064406

15. Moskvin E, Grigoriev S, Dyadkin V, Eckerlebe H, Baenitz M, Schmidt M, et al. Complex Chiral Modulations in Fege Close to Magnetic Ordering. *Phys Rev Lett* (2013) 110:077207. doi:10.1103/PhysRevLett.110.077207

16. Seki S, Kim J-H, Inosov DS, Georgii R, Keimer B, Ishiwata S, et al. Formation and Rotation of Skyrmion crystal in the Chiral-Lattice Insulator Cu2oseo3. *Phys Rev B* (2012) 85:220406. doi:10.1103/physrevb.85.220406

17. Bak P, and Jensen MH. Theory of Helical Magnetic Structures and Phase Transitions in Mnsi and Fege. *J Phys C: Solid State Phys* (1980) 13:L881–L885. doi:10.1088/0022-3719/13/31/002

18. Park J-H, and Han JH. Zero-temperature Phases for Chiral Magnets in Three Dimensions. *Phys Rev B* (2011) 83:184406. doi:10.1103/physrevb.83.184406

19. Halder M, Chacon A, Bauer A, Simeth W, Mühlbauer S, Berger H, et al. Thermodynamic Evidence of a Second Skyrmion Lattice Phase and Tilted Conical Phase in Cu2oseo3. *Phys Rev B* (2018) 98:144429. doi:10.1103/physrevb.98.144429

20. Chacon A, Heinen L, Halder M, Bauer A, Simeth W, Mühlbauer S, et al. Observation of Two Independent Skyrmion Phases in a Chiral Magnetic Material. *Nat Phys* (2018) 14:936–41. doi:10.1038/s41567-018-0184-y

21. Luo Y, Lin S-Z, Fobes DM, Liu Z, Bauer ED, Betts JB, et al. Anisotropic Magnetocrystalline Coupling of the Skyrmion Lattice in Mnsi. *Phys Rev B* (2018) 97:104423. doi:10.1103/physrevb.97.104423

22. Shibata K, Iwasaki J, Kanazawa N, Aizawa A, Tanigaki T, Shirai M, et al. Large Anisotropic Deformation of Skyrmions in Strained crystal. *Nat Nanotech* (2015) 10:589–92. doi:10.1038/nnano.2015.113

23. Wang C, Du H, Zhao X, Jin C, Tian M, Zhang Y, et al. Enhanced Stability of the Magnetic Skyrmion Lattice Phase under a Tilted Magnetic Field in a Two-Dimensional Chiral Magnet. *Nano Lett* (2017) 17:2921–7. doi:10.1021/acs.nanolett.7b00135

24. Makino K, Reim JD, Higashi D, Okuyama D, Sato TJ, Nambu Y, et al. Thermal Stability and Irreversibility of Skyrmion-Lattice Phases in Cu2oseo3. *Phys Rev B* (2017) 95:134412. doi:10.1103/physrevb.95.134412

25. Grigoriev SV, Potapova NM, Moskvin EV, Dyadkin VA, Dewhurst C, and Maleyev SV. Hexagonal Spin Structure of A-phase in Mnsi: Densely Packed Skyrmion Quasiparticles or Two-Dimensionally Modulated Spin Superlattice?. *Jetp Lett* (2014) 100:216–21. doi:10.1134/s0021364014150065

26. Bannenberg LJ, Qian F, Dalgliesh RM, Martin N, Chaboussant G, Schmidt M, et al. Reorientations, Relaxations, Metastabilities, and Multidomains of Skyrmion Lattices. *Phys Rev B* (2017a) 96:184416. doi:10.1103/physrevb.96.184416

27. Adams T, Mühlbauer S, Neubauer A, Münzer W, Jonietz F, Georgii R, et al. Skyrmion Lattice Domains in Fe1−xCoxSi. *J Phys Conf Ser* (2010) 200:032001. doi:10.1088/1742-6596/200/3/032001

28. Bannenberg LJ, Kakurai K, Qian F, Lelièvre-Berna E, Dewhurst CD, Onose Y, et al. Extended Skyrmion Lattice Scattering and Long-Time Memory in the Chiral magnetFe1−xCoxSi. *Phys Rev B* (2016) 94:104406. doi:10.1103/physrevb.94.104406

29. Bannenberg LJ, Kakurai K, Falus P, Lelièvre-Berna E, Dalgliesh R, Dewhurst CD, et al. Universality of the Helimagnetic Transition in Cubic Chiral Magnets: Small Angle Neutron Scattering and Neutron Spin echo Spectroscopy Studies of Fecosi. *Phys Rev B* (2017b) 95:144433. doi:10.1103/physrevb.95.144433

30. Wan X, Hu Y, and Wang B. Exchange-anisotropy-induced Intrinsic Distortion, Structural Transition, and Rotational Transition in Skyrmion Crystals. *Phys Rev B* (2018) 98:174427. doi:10.1103/physrevb.98.174427

31. Hu Y. Wave Nature and Metastability of Emergent Crystals in Chiral Magnets. *Commun Phys* (2018) 1:82. doi:10.1038/s42005-018-0071-y

32. Hu Y, and Wan X. Thermodynamics and Elasticity of Emergent Crystals. *arXiv:1905.02165* (2019).

33. Reichhardt C, Reichhardt C, and Milosevic M. Statics and Dynamics of Skyrmions Interacting with Pinning: A Review. *arXiv:2102.10464* (2021).

34. Hu Y, and Wang B. Unified Theory of Magnetoelastic Effects in B20 Chiral Magnets. *New J Phys* (2017) 19:123002. doi:10.1088/1367-2630/aa9507

35. Ehlers D, Stasinopoulos I, Kézsmárki I, Fehér T, Tsurkan V, von Nidda H-AK, et al. Exchange Anisotropy in the Skyrmion Host Gav4s8. *J Phys Condens Matter* (2016) 29:065803. doi:10.1088/1361-648x/aa4e7e

36. Adams T, Mühlbauer S, Pfleiderer C, Jonietz F, Bauer A, Neubauer A, et al. Long-range Crystalline Nature of the Skyrmion Lattice in Mnsi. *Phys Rev Lett* (2011) 107:217206. doi:10.1103/physrevlett.107.217206

37. Grigoriev S, Maleyev S, Dyadkin V, Menzel D, Schoenes J, and Eckerlebe H. Principal Interactions in the Magnetic System Fe1−xcoxsi: Magnetic Structure and Critical Temperature by Neutron Diffraction and Squid Measurements. *Phys Rev B* (2007) 76:092407. doi:10.1103/physrevb.76.092407

38. Takeda M, Endoh Y, Kakurai K, Onose Y, Suzuki J, and Tokura Y. Nematic-to-smectic Transition of Magnetic Texture in Conical State. *J Phys Soc Jpn* (2009) 78:093704. doi:10.1143/jpsj.78.093704

39. Bannenberg LJ, Wilhelm H, Cubitt R, Labh A, Schmidt MP, Lelièvre-Berna E, et al. Multiple Low-Temperature Skyrmionic States in a Bulk Chiral Magnet. *Npj Quan Mater.* (2019) 4:11. doi:10.1038/s41535-019-0150-7

40. Qian F, Bannenberg LJ, Wilhelm H, Chaboussant G, Debeer-Schmitt LM, Schmidt MP, et al. New Magnetic Phase of the Chiral Skyrmion Material Cu2oseo3. *Sci Adv* (2018) 4:eaat7323. doi:10.1126/sciadv.aat7323

41. Wan X, Hu Y, and Wang B. First and Second Order Rotational Transitions of Skyrmion crystal in Multiferroic Cu2oseo3 under Electric Field. *Appl Phys Lett* (2020) 116:182403. doi:10.1063/5.0003880

42. White JS, Prša K, Huang P, Omrani AA, Živković I, Bartkowiak M, et al. Electric-Field-Induced Skyrmion Distortion and Giant Lattice Rotation in the Magnetoelectric InsulatorCu2OSeO3. *Phys Rev Lett* (2014) 113:107203. doi:10.1103/physrevlett.113.107203

43. Leonov AO, and Kézsmárki I. Skyrmion Robustness in Noncentrosymmetric Magnets with Axial Symmetry: The Role of Anisotropy and Tilted Magnetic fields. *Phys Rev B* (2017) 96:214413. doi:10.1103/physrevb.96.214413

44. Kézsmárki I, Bordács S, Milde P, Neuber E, Eng LM, White JS, et al. Néel-type Skyrmion Lattice with Confined Orientation in the Polar Magnetic Semiconductor GaV4S8. *Nat Mater* (2015) 14:1116–22. doi:10.1038/nmat4402

45. Kurumaji T, Nakajima T, Ukleev V, Feoktystov A, Arima T-h., Kakurai K, et al. Néel-Type Skyrmion Lattice in the Tetragonal Polar Magnet VOSe2O5. *Phys Rev Lett* (2017) 119:237201. doi:10.1103/physrevlett.119.237201